Cerebral Cortex January 2013;23:36–48
doi:10.1093/cercor/bhr372
Advance Access publication January 23, 2012

Diffusion Tensor Imaging–Based Characterization of Brain Neurodevelopment in Primates

Yundi Shi[1], Sarah J. Short[1], Rebecca C. Knickmeyer[1], Jiaping Wang[2], Christopher L. Coe[3], Marc Niethammer[2], John H. Gilmore[1], Hongtu Zhu[4] and Martin A. Styner[1,2]

[1]Department of Psychiatry, [2]Department of Computer Science, University of North Carolina, Chapel Hill, NC 27599-7160, USA, [3]Department of Psychology, Harlow Center, University of Wisconsin, Madison, WI 53706-1611, USA and [4]Department of Biostatistics, University of North Carolina, Chapel Hill, NC 27599-7160, USA

Address correspondence to Yundi Shi, Department of Psychiatry, 355 Medical School Wing C, University of North Carolina at Chapel Hill, Chapel Hill, NC 27599-7160, USA. Email: yundiuu@gmail.com.

Primate neuroimaging provides a critical opportunity for understanding neurodevelopment. Yet the lack of a normative description has limited the direct comparison with changes in humans. This paper presents for the first time a cross-sectional diffusion tensor imaging (DTI) study characterizing primate brain neurodevelopment between 1 and 6 years of age on 25 healthy undisturbed rhesus monkeys (14 male, 11 female). A comprehensive analysis including region-of-interest, voxel-wise, and fiber tract–based approach demonstrated significant changes of DTI properties over time. Changes in fractional anisotropy (FA), mean diffusivity, axial diffusivity (AD), and radial diffusivity (RD) exhibited a heterogeneous pattern across different regions as well as along fiber tracts. Most of these patterns are similar to those from human studies yet a few followed unique patterns. Overall, we observed substantial increase in FA and AD and a decrease in RD for white matter (WM) along with similar yet smaller changes in gray matter (GM). We further observed an overall posterior-to-anterior trend in DTI property changes over time and strong correlations between WM and GM development. These DTI trends provide crucial insights into underlying age-related biological maturation, including myelination, axonal density changes, fiber tract reorganization, and synaptic pruning processes.

Keywords: atlas, brain development, diffusion tensor imaging, rhesus, tractography

Introduction

Our current understanding of neurodevelopment is still limited with respect to the trajectories of white matter (WM) maturation. Diffusion tensor imaging (DTI) enables characterization of WM properties and growth of brain structures and the fiber tracts that connect them. The current study provides the first analysis of WM development spanning 1–6 years of age in a nonhuman primate species and explored the potential use of DTI as a tool for tracking gray matter (GM) progression. This developmental window captures one of the most formative and poorly characterized periods of neural maturation in both humans and nonhuman primates. Using 3 complementary analytic approaches, we sought to discern patterns of neurodevelopment in the typically maturing primate brain. A more detailed understanding of normal neural development provides the essential framework to allow further insights into the pathology of neurodevelopmental disorders, which can be usefully modeled, in nonhuman primates.

Brain maturation is a complex process driven by myelination, growth of neurons, and of their connections during the first years of life. The increase in neural connections is followed by a subsequent process of dendritic pruning and loss of synaptic contacts, presumably achieving a more efficient network of connections that continue to be remodeled throughout life (Dawson and Fischer 1994; Engert and Bonhoeffer 1999; Stepanyants et al. 2002; Lebel et al. 2008). Although brain maturation has been studied extensively, both at the phenotypic level (behavior) and at the low substrate level (cellular anatomy and physiology), information at the level of neuroanatomical connectivity, including the maturational changes during the prepubertal years, remains sparse. However, this information is of special interest because it provides insight into the anatomical substrates and the timing of brain changes and helps to account for shifts in function during development. Understanding developmental brain changes will ultimately facilitate better diagnoses and the refinement of targeted therapies for neurodevelopmental and psychiatric brain disorders.

Nonhuman primate models are widely used to generate comparative information associated with human neuropathology (Glatzel et al. 2002; Grant and Bennett 2003; Machado and Bachevalier 2003; Lebherz et al. 2005; Sullivan et al. 2005; Barr and Goldman 2006; Lubach and Coe 2006; Segerstrom et al. 2006; Bennett 2008; Williams et al. 2008). Among the many nonhuman primate species, the rhesus macaque (*Macaca mulatta*) has been the most widely used monkey to investigate the neural substrates of human behavior, due to its phylogenetic closeness to humans (Lacreuse and Herndon 2009), the long-standing domestic breeding programs, and the potential to examine more complex cognitive functions and social behavior in this intelligent and gregarious animal (Amaral 2002). In addition, rhesus macaques show hemispheric asymmetry and sex differences during the pubertal period that parallel ones seen in humans (Giedd et al. 1999; Buchel et al. 2004; Gong et al. 2005). For more than 40 years, this species has been used to evaluate how disturbances of the early rearing environment can induce behavioral abnormalities (Harlow et al. 1971). The relevance of this animal model extends beyond biological similarities. Like humans, nonhuman primates have a protracted developmental trajectory that is characterized by complex social and emotional underpinnings. As such, characterization of normal brain development in the rhesus macaque is necessary to identify these similarities and differences between the humans and the macaque and to better align the maturational changes associated with the critical transitional period of puberty.

Nevertheless, only a few DTI studies of nonhuman primates exist. In macaques, Makris et al. (2007) investigated changes in WM fiber bundles with aging. They reported reductions in fractional anisotropy (FA) in corticocortical association fibers with age (7–31 years of age), which were in general agreement

with observations in humans (ca. corresponds to 20–90 years of age). Our previous studies (Styner et al. 2007, 2008) explored changes in the developing macaque brain using an atlas-driven brain parcellation and showed increases in FA, particularly in the corpus callosum (CC), as well as decreases in mean diffusivity (MD). Combining structural magnetic resonance imaging (MRI) and DTI is particularly useful to investigate brain maturation over the full range of neurodevelopment. While contrasts in WM are difficult to analyze with structural MRI at early stages of brain development, the integrity of WM can be characterized with DTI.

This paper extends our previous work (Styner et al. 2007, 2008; Short et al. 2010), which established the framework to perform atlas building and atlas-based automatic brain analysis. The results of 3 atlas-based DTI analysis approaches are presented, with each analytic step having a different advantages and limitations. We start with a coarse-scale regional analysis (similar to D'Arceuil et al. 2007), which has high stability but lumps together different fiber tracts running through the same region. Then, a fine-scale voxel-wise analysis (Makris et al. 2007; Liu et al. 2009) was performed that allows a more detailed representation of the changes across time but is susceptible to small registration errors, as well as more sensitive to noise. Finally, a fiber tract–based analysis (Parker et al. 2002; Croxson et al. 2005; Zhu et al. 2010) allowed us to analyze DTI properties along the tracts and provided us with an intermediate scale analysis as compared with the prior 2 steps (Fig. 1). To our knowledge, this is the first systematic DTI study of nonhuman primate neurodevelopment.

Materials and Methods

Subjects

Twenty-five healthy, nonhandled rhesus monkeys (14 male, 11 female) between the ages of 319 days (ca. 1 year) and 2144 days (ca. 6 years) (Table 1) were generated from a large (500+) monkey breeding colony at the Harlow Primate Laboratory (University of Wisconsin, Madison, WI). The animals came from known pedigrees with clinical and family histories extending back 8 generations and over 50 years. As previous studies suggested (Makris et al. 2007), the ratio of monkey to human age is approximately 1:3, thus the subjects in this study parallel humans with the age of about 3–18. The cohort of monkeys used for these MRI analyses were offsprings from 25 healthy, multiparous females that had been born and raised normally at the same facility. There were also no manipulations of the gravid female during the course of pregnancy. All monkeys were reared and housed in standardized conditions. Infants were reared by the mother until 6–8 months of age and then weaned into small social groups, each comprised of 4–8 animals. Subadult animals were housed in mixed-age groups or as social pairs with another animal of the same age and sex. Thus, all animals scanned for

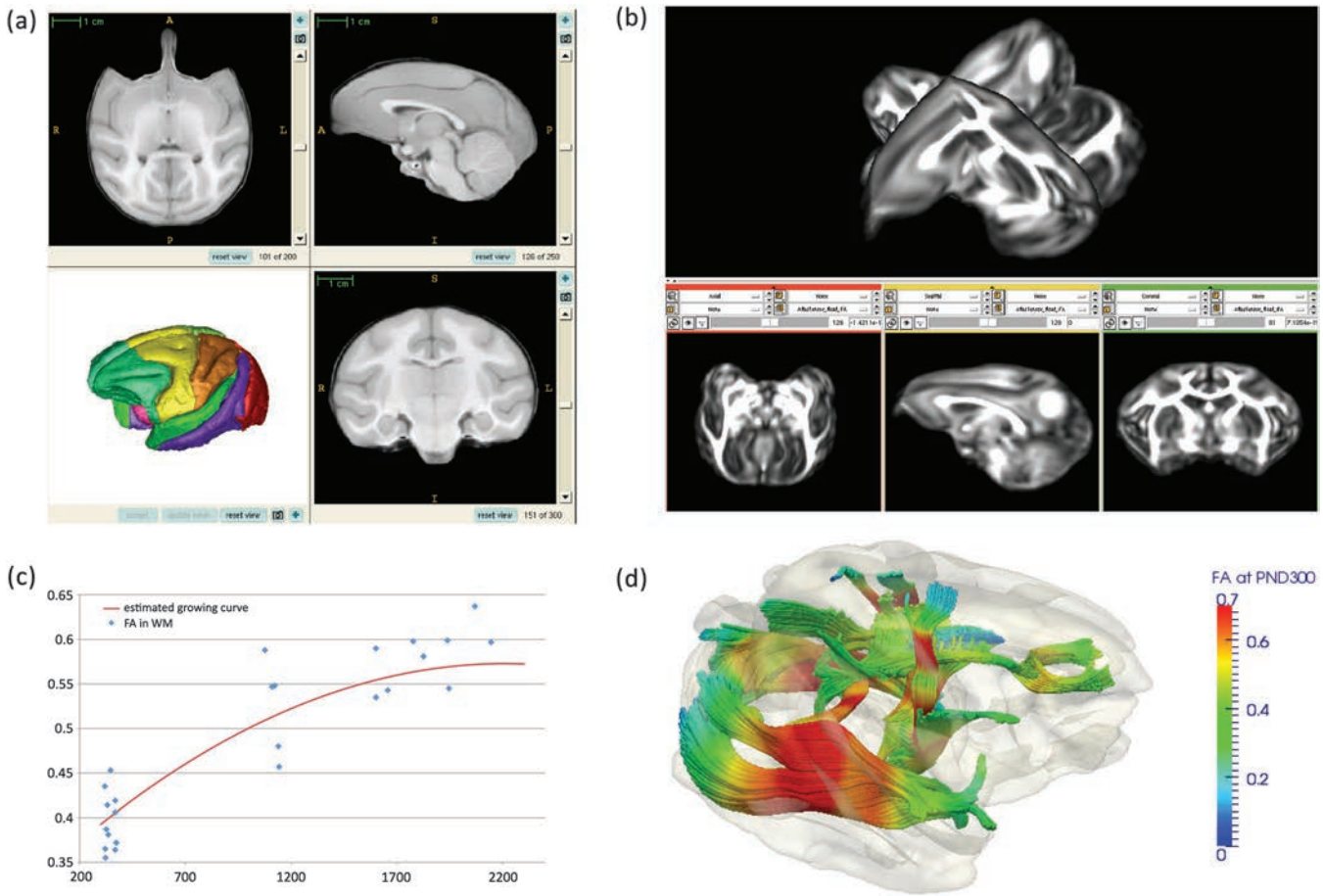

Figure 1. Pipeline of the atlas-based study. (*a*) A structural atlas was constructed using T_1 images, and different lobar parcellations were defined on this atlas. (*b*) A corresponding DTI atlas was created with FA images coregistered to T_1 images. (*c*) ROI-based statistical analysis was performed for each lobar parcellation using a linear growth model. FA curve in the corpus callosum is shown as an example. Tract-based analysis was similar to ROI analysis (*c*) with the exception that statistical modeling of diffusion properties was done for each sampling point along the fiber instead of in each parcellation ROI. (*d*) All the fiber tracts included in this study including the genu, the cingulum, the inferior longitudinal fasciculus, different subdivisions of the internal capsule, and the splenium. Fiber tracts were colored by the FA values at postnatal day (PND) 300.

Table 1
Age and gender information of the subjects

Age range	Number of female	Number of male
300–900 days	5	6
900–1500 days	3	2
1500–2200 days	6	3

Note: Younger ages are overrepresented as we suspected the brain changes more rapidly during this time.

this project had been socially reared, maintained in a controlled manner, and free of experimental manipulations that might alter brain development. Animals were fed a standardized diet of commercial biscuits (Teklad, Harlan Laboratories, Madison, WI) and provided fruit supplements and foraging devices for enrichment. Water was available ad libitum, temperature controlled at 23 °C, and the light:dark cycle maintained at 14:10 with lights on at 06:00 AM. The housing conditions and experimental procedures were approved by the Institutional Animal Care and Use Committee of the University of Wisconsin-Madison.

MRI Acquisition

All subjects were scanned on a GE Signa 3-T scanner (General Electric Medical Systems, Milwaukee, WI) at the Waisman Center. T_1-weighted images were acquired using a high-resolution axial 3D-SPGR sequence (time repetition [TR] = 8.6 ms, time echo [TE] = 2.0 ms, Field of View (FOV) = 14 cm, flip angle = 10°, matrix = 512 × 512, voxel size = 0.27 mm, slice thickness = 1 mm, slice gap = 0.5 mm, bandwidth = 15.63) with an effective voxel resolution of 0.27 × 0.27 × 0.5 mm^3. Spin-echo sequence was performed to acquire T_2-weighted images (TR = 12 000 ms, TE = 90 ms, FOV = 14 cm, flip angle = 90°, matrix = 512 × 512, voxel size = 0.27 mm^3, slice thickness = 1.5 mm, slice gap = 0 mm, bandwidth = 31.25). Diffusion-weighted images (DWIs) were acquired using an echo planar imaging (EPI) sequence (0.55 × 0.55 × 2.5 mm^3) with 12 unique directions at b = 1000 s/mm^2 and a single base image at b = 0. The in-plane resolution was upsampled in K-space by a factor of 2 on the scanner. Ketamine hydrochloride (10 mg/kg Intra-muscular (I.M.)) followed by medatomidine (50 μg/kg I.M.) was used for immobilization during scanning. All younger monkeys were oriented identically within a stereotaxic platform, the larger 4–6 years old subadults were oriented in the same plane on a stabilizing pillow; all within a standard 18-cm-diameter quadrature extremity coil. Similar orientation and the absence of marked head tilt or yaw were verified in the sagittal and coronal planes on the scanner.

Tensor Estimation and Diffusion Properties Computation

DWIs were upinterpolated to an isotropic 0.55 mm resolution using windowed sinc interpolation. Diffusion tensors were computed using weighted least squares fitting (Goodlett et al. 2009) via the NA-MIC DTI Process software suite (http://www.nitrc.org/projects/dtiprocess). Eigenvalues $(\lambda_1 \geqslant \lambda_2 \geqslant \lambda_3)$ and corresponding eigenvectors were calculated to obtain the diffusion properties, including FA, MD, axial diffusivity (AD), and radial diffusivity (RD), where $\mathrm{FA} = \sqrt{\frac{1}{2}}\sqrt{\frac{(\lambda_1-\lambda_2)^2+(\lambda_1-\lambda_3)^2+(\lambda_2-\lambda_3)^2}{\lambda_1^2+\lambda_2^2+\lambda_3^2}}$, $\mathrm{MD} = \frac{1}{3}(\lambda_1+\lambda_2+\lambda_3)$, $\mathrm{AD} = \lambda_{\|} = \lambda_1$, $\mathrm{RD} = \lambda_{\perp} = \frac{1}{2}(\lambda_2+\lambda_3)$. AD shows parallel diffusivity and increases with refined microorganization and maturation, while RD measures perpendicular diffusivity and decreases with axonal myelination (Zhang et al. 2009). MD represents the average total diffusion, while FA is a measure similar to the ratio between parallel and perpendicular diffusion. Both refined organization (increase of AD) or a higher degree of myelination (decrease of RD) lead to higher values of FA. These diffusion properties well characterize the local microorganization in WM but also possibly in GM areas. Skull stripping was performed by applying a binary brain mask to the diffusion property maps. For each subject, T_1-weighted image was registered to the corresponding FA map, and a structural brain mask generated with atlas-based automatic tissue segmentation (Styner et al. 2007) was propagated with this transformation to generate the DTI brain mask.

Regional ROI-Based Analysis

Regional analysis is currently the most common approach employed in DTI studies. We performed a fully automatic regional analysis using coregistered tissue and lobar segmentations that were computed on corresponding structural MRIs. Median values of the diffusion properties in each parcellation region were computed for WM and GM tissues. Changes over time were analyzed statistically to quantitatively characterize the developmental pattern of FA, MD, AD, and RD for each region and to detect differences among these regions. This method can be applied in a straightforward manner for large-scale analyses and allows the application of standardized statistical methods. While this analysis step has the advantage of being stable and having a robust tolerance for noise and minor registration errors, it does not separate fiber tracts within the same region that potentially develop differently, such as the genu tract and uncinate fasciculus both of which are found in the prefrontal lobe.

Brain Tissue Classification and Lobar Parcellation

In our earlier work (Styner et al. 2007), we generated coregistered unbiased, structural T_1- and T_2- weighted atlases using training animal scans in the age range of 16–34 months (http://www.nitrc.org/projects/primate_atlas). Probabilistic maps for WM, GM, and cerebrospinal fluid (CSF) were defined on the atlas alongside lobar parcellations and subcortical brain structures. Parcellations and structures were determined manually using the ITK-SNAP segmentation tool (Yushkevich et al. 2006) (http://www.itksnap.org/download/snap). The full parcellation consisted of the left and right hemisphere of the prefrontal, frontal, cingulate, corpus callosum, parietal, temporal auditory, temporal visual, temporal limbic, and occipital lobes as well as the cerebellum, subcortical structure, and brainstem (Styner et al. 2007, 2008) (https://www.ia.unc.edu/dev/tutorials).

Coregistered DTI Property Computation

T_1- and T_2- weighted images were registered to the FA image via normalized mutual information-based b-spline registration (Rueckert et al. 1999) in a two-step process (http://www.doc.ic.ac.uk/~dr/software) for each subject. All images were skull-stripped prior to the registration process. As a first step, the T_2-weighted image was registered to the b = 0 image using a uniform 4 mm spacing of the b-spline control points. Next, this registration was refined by matching the T_1-weighted image with the FA image. Subsequently, the full registration was applied to both the probabilistic WM/GM segmentations and the parcellation maps. The registered WM and GM maps were finally masked with all the parcellations. Next, the median of FA, MD, AD, and RD were computed within each parcellation for every subject. For the WM, bilateral parcellations included the left and right lobes of prefrontal (PF), frontal (FT), cingulate (CG), corpus callosum (CC), parietal (PT), temporal auditory (TA), temporal visual (TV), temporal limbic (TL), occipital (OC), cerebellum (CB), as well as the pons and medulla (PM). Analyses of GM were performed on the same lobar parcellations although the GM structure like the insula (IL) was included in the analysis, while some WM regions such as the CC and PM were excluded.

Regional Statistical Analysis

As mentioned above, we employed the median values of the diffusion properties rather than the arithmetic mean as it is considered to be less sensitive to noise, registration, and segmentation errors. All statistical analyses for region of interest–based data were performed using PROC Mixed in SAS 9.2 (SAS Institute Inc, Cary, NC). A linear growth model was used to delineate the trajectory of changes for diffusion properties in each ROI using DTI data between 10 and 72 months. Multiple diffusion properties at each ROI were simultaneously entered into the linear growth model as a multivariate outcome-dependent vector. The linear and quadratic terms of age were then included as fixed effects to model the mean trajectory of each diffusion property as a function of age. An unstructured correlation structure was employed to model correlation among different diffusion properties. The F-test statistic was used to test the null hypothesis that both age and age square terms equal zero for statistically examining the Age effect. The possible

influence of gender was considered in the initial statistical analyses, although with this number of subjects, we did not observe any significant differences between males and females.

DTI Atlas Building for Voxel-Wise and Fiber Tract–Based Analysis

We computed a DTI atlas in order to map all individual DTI data to a common coordinate system enabling tract-based and voxel-based analysis. Seventy-nine subjects were used to construct this atlas including all the normal control subjects from this study as well as additional monkeys from handled subjects in an intrauterine flu-exposure study (Knickmeyer et al. 2010; Short et al. 2010). A large number of subjects were included to achieve a desirable signal-to-noise ratio (SNR) in the atlas. All the subjects had no major pathology and share the same morphometric appearance. The same basic algorithm used for the structural atlas computation was also used to build an unbiased atlas (Joshi et al. 2004) of FA yielding diffeomorphic field maps that warp each individual subject to the atlas. These field maps were then applied to each corresponding tensor image, and a finite-strain algorithm was adopted to reorient the tensors (Alexander et al. 2001). The DTI atlas was finally computed as the average of all of these warped tensor images (Goodlett et al. 2009). A similar atlas (Adluru et al. 2012) has recently become publicly available from our collaborating group.

Voxel-Wise Analysis

Voxel-wise analysis determines the change of each voxel over time without assumptions of specific tract geometry or human interaction (i.e., ROI labeling or fiber tracking). A multiscale adaptive model (MARM)–based on generalized estimation equations was developed to spatially and adaptively analyze imaging measures across all voxels (Zhu et al. 2009; Li et al. 2011). Common existing voxel-wise approaches often treat all voxels as independent units and employ local smoothing operations for spatial coherence. We refined an MARM to avoid such deficits by accounting for the spatial correlation as well as preserving tissue boundaries because the initial smoothing step often dramatically increases the numbers of false positives and false negatives. Specifically, at each voxel, we fit a linear regression model with each diffusion property as an outcome dependent variable, as well as gender and the linear and quadratic terms of age as fixed effects. Sequentially, our multiscale adaptive estimation and testing procedure were used to incorporate the neighboring information from each voxel to adaptively calculate parameter estimates and test statistics. Finally, false discovery rate (FDR) correction (Genovese et al. 2002) was used to correct for multiple comparisons. It is an excellent way to pursue localized hypothesis generating and provides detailed information complementary to ROI-based and tract-based analysis.

Fiber Tract–Based Analysis

The study of atlas-based DTI properties as a function of arc length along a DTI streamline fiber tract is becoming an important source of information for investigating neurodevelopment (Ding et al. 2003; Corouge et al. 2006; Fletcher et al. 2007; Goodlett et al. 2009). In our work, we performed fiber tracking in the DTI atlas space with Slicer3 (http://www.slicer.org). Recent studies in macaque highlighted the validity of the tested tractography methods to reliably recover major fiber bundles by demonstrating good agreement for major fiber bundles to histology sections stained by a neural tracer (Dauguet et al. 2006, 2007). ROI seeding voxels were manually determined, and a standard streamline algorithm was used to obtain the major fiber tracts, including the genu, the cingulum, the inferior longitudinal fasciculus, different subdivisions of the internal capsule, and the splenium. These fibers were then sampled with an arc length of 0.5 mm in the atlas. Diffusion properties, including FA, MD, AD, and RD, were computed at these sampling points for each subject, which had been warped into the atlas space in the atlas-building step. The median was calculated at corresponding sampling points across the fiber bundles yielding a single profile along the tract for each fiber bundle (Goodlett et al. 2009). Previous studies have shown that the median is more robust to noise and variability in fiber-tracking as compared with the arithmetic mean.

Fiber Tract–Based Statistical Analysis

The FRATS fiber tract analysis framework (Zhu et al. 2010, 2011) was applied to compute the change of FA, MD, AD, and RD along each fiber tract across time. FRATS first employed a local polynomial kernel method for jointly smoothing multiple diffusion properties along individual fiber bundles. Then a functional linear regression model was used for characterizing the association between the fiber bundle diffusion properties and the 3 covariates: gender, linear, and quadratic age terms. Local and global test statistics were additionally estimated to test for age effects.

Results

ROI

In general, significant changes in all diffusion properties over time were observed in all lobar parcellations for both WM and GM (P values from multitesting < 0.01). Similar patterns of temporal change for WM and GM were detected in FA, MD, AD, and RD (Fig. 2), although changes in WM occurred on a greater scale when compared with GM.

DTI Development in WM

As expected, FA increased prominently over time in all regions. Regions that showed a particularly substantial increase included the cingulate, temporal visual, occipital lobe, and corpus callosum (Figs 2 and 3). The increase was more pronounced at younger ages (from 300 to 900 days) and tapered off with the maturation of the brain. At 300 days, FA followed an anterior to posterior gradient, being highest in the prefrontal and frontal regions and lowest in the occipital region. FA in the prefrontal, frontal, parietal, and occipital lobes all attained similar values by young adulthood, whereas FA values in the auditory temporal lobe still remained relatively low. A greater degree of change occurred in the occipital lobes than in the prefrontal and frontal lobes between 300 days (about 1 year) to 1500 days (about 3 years). AD values increased as RD values decreased over time in most of the regions. The regions that revealed the most increase in AD were the pons and medulla, the cingulate cortex, and the corpus callosum. The largest decrease in RD was present in corpus callosum and cingulate. For most regions, the decrease in RD was also greater than the increase in AD, resulting in an overall decrease of the MD except for the left hemisphere of temporal limbic lobe. Asymmetric values as well as asymmetric development were observed in the left and right hemisphere for all diffusion properties.

DTI Development in GM

FA values for the GM were notably lower than for the WM, as expected. Most regions showed a significant overall increase in FA, except for the cingulate cortex and the right hemisphere of the prefrontal region (Figs 2 and 4). Both hemispheres of the prefrontal region evinced a decrease in FA from 300 to 900 days and a slight increase from 900 to 1500 days. The occipital regions and the cerebellum showed the most increase in FA when compared with all other parcellated lobes. Changes of AD in GM were marginal in most of the regions. Of the 20 regions analyzed, 11 showed increased AD and 9 had decreased AD. RD decreased slightly for most of the regions except for the temporal limbic region and occipital lobes bilaterally. MD showed the same pattern of change as RD. Furthermore, we investigated whether DTI development in WM and GM were correlated. The observed changes of FA, MD, and RD indicated

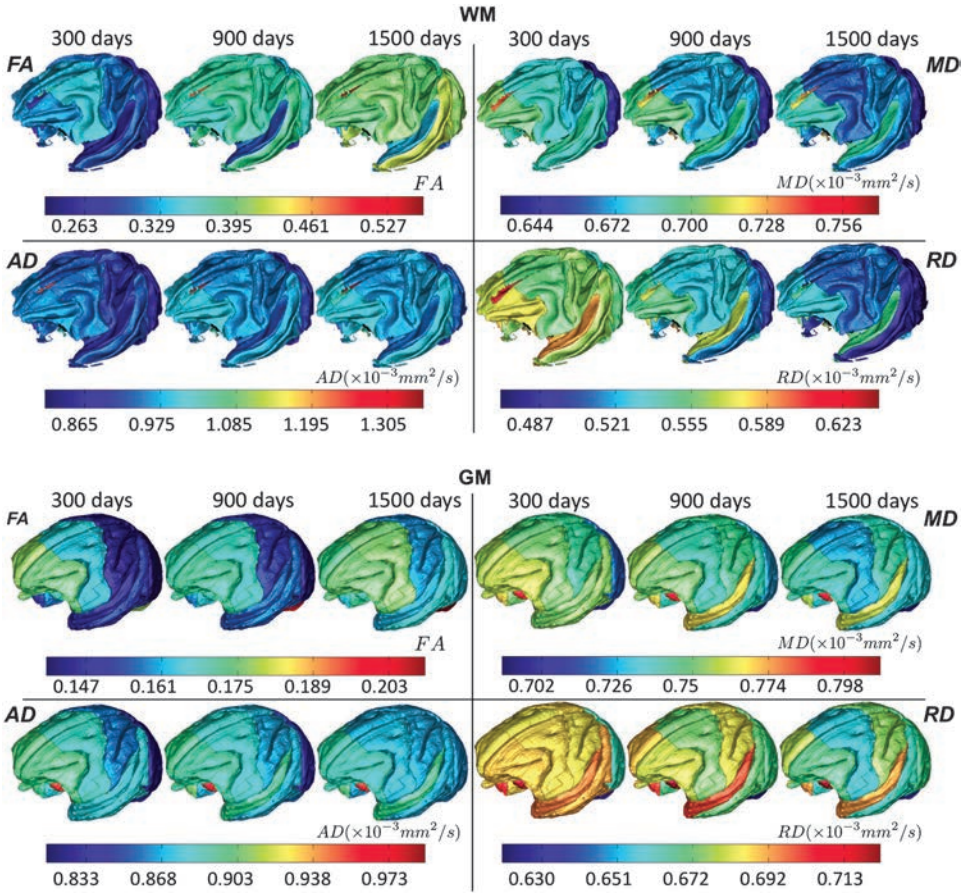

Figure 2. Estimation of FA, MD, AD, and RD using ROI-based generalized linear model (GLM) at age 300, 900, and 1500 days (ca. 1, 2.5 and 4 years old) for WM and GM, respectively. Visualization was chosen to illustrate the cortical regions of the left hemisphere. Note that color scales were chosen independently for WM and GM to aid visual differentiation of changes over time in different lobar regions. For detailed results for all regions and comparisons between WM and GM, please refer to Figures 3 and 4.

that there was a strong correlation between WM and GM (Fig. 5), while changes of AD suggested that there was little association between WM and GM for this parameter.

Voxel-Wise Analysis (VBA)

Voxels with significant development over time (P value < 5%) have been highlighted using MARM (Fig. 6). Connected components of small size were rejected to reduce false positives. A CSF mask was also applied to exclude CSF and skull regions. Overall, 44.84% of the brain volume (CSF excluded) showed significant changes in FA, while changes of 24.85%, 29.64%, and 33.01% were seen for MD, AD, and RD, respectively. In order to assess the consistency across analytic methods, we overlaid the VBA-based results with those from the tract-based approach. In general, we observed that those regions demonstrating significant change in the VBA-based results also showed a similarly significant change in the tract-based approach. However, we did find several regions of significant changes in the tract-based approach without corresponding significant changes in the VBA. This outcome is not surprising, as VBA methods in general suffer from limited sensitivity.

Fiber Tract

A global (cumulative) P value for each fiber tract was generated using our statistical fiber analysis framework FRATS (Table 2). Most of the fiber tracts showed significant changes over time for all diffusion properties. FA presented significant changes in all the fiber tracts that were a focus of this study (genu, splenium, cingulum, inferior longitudinal fasciculus (ILF), and internal capsule in the left and right hemisphere). Tracts that showed global significant changes in all diffusion properties are cingulum, thalamic radiation to the prefrontal region, from pons to the right parietal region, and the splenium. In addition, MD and RD in the genu showed significant changes over time, while the change in AD was not significant across the studied age range.

Localized significant changes are clearly visible in Figs 7 and 8. Considerable increases of FA over time are visible in all tracts. The splenium, in contrast to the genu, showed increases in FA and decreases in RD earlier in time, that is, mostly between 1 and 3 years as compared with 3–5 years. AD showed increase in all tracts while RD showed decrease. The RD decrease in the splenium was minimal compared with the internal capsule tracts and the genu. MD in the splenium and internal capsule all showed increases, in contrast to the decreased MD found in the genu.

Discussion

To our knowledge, this is the first DTI-based study to characterize normal development in nonhuman primates from late infancy to early adulthood period. It provided

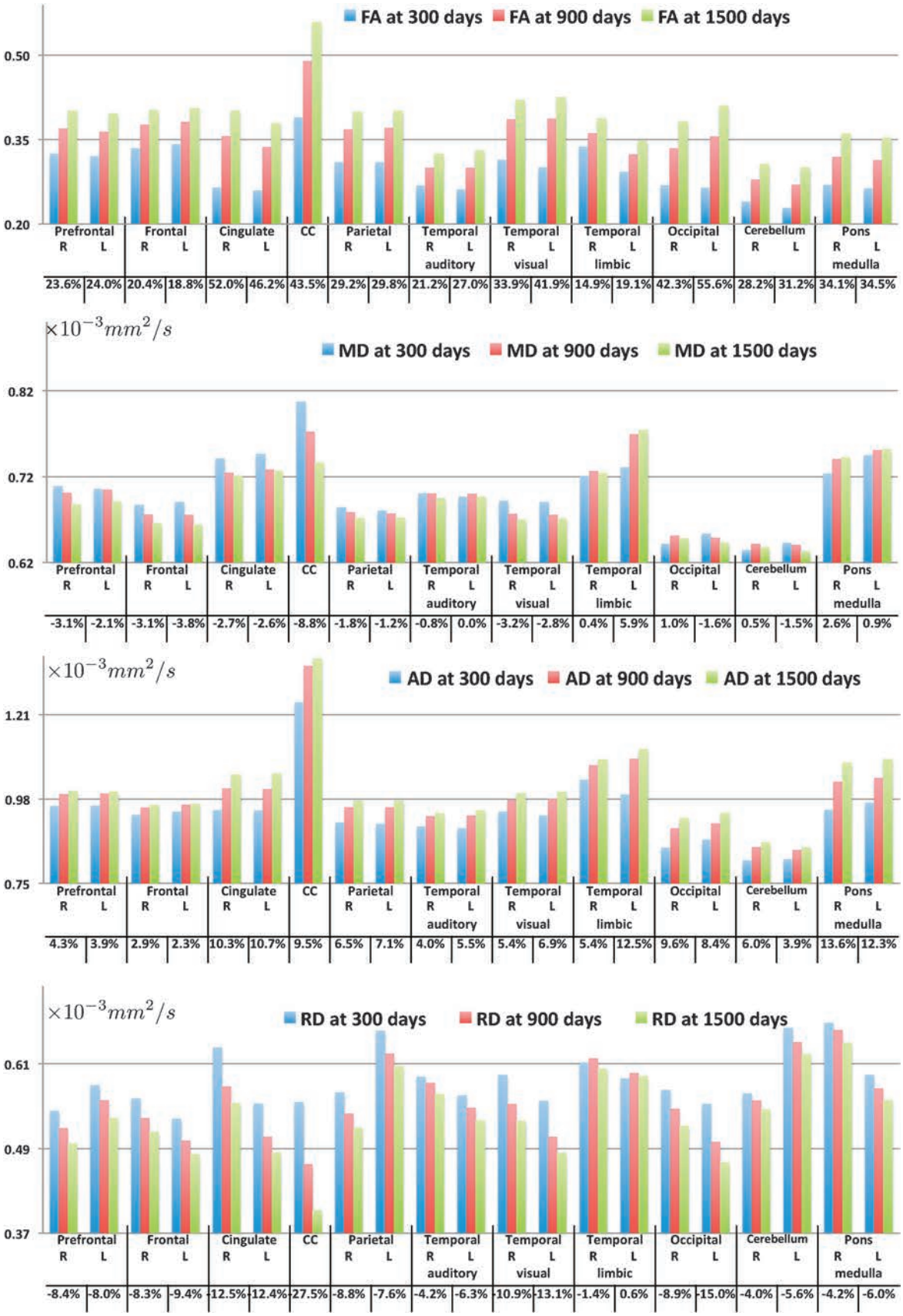

Figure 3. Estimation of FA, MD, AD, and RD for all the ROIs in WM at age 300, 900, and 1500 days using the linear growth model. Overall changes from 300 to 1500 days are shown as percentages.

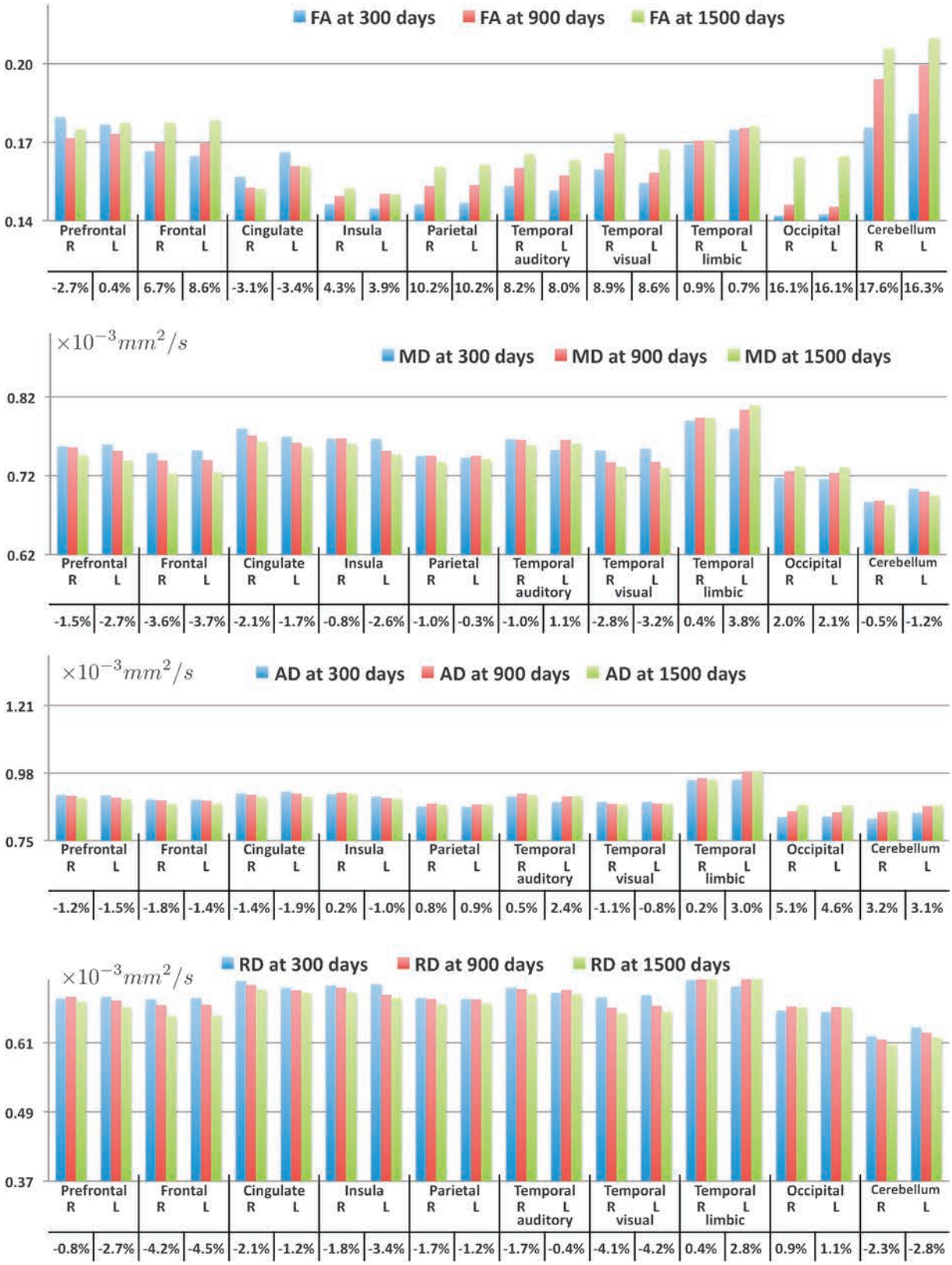

Figure 4. Estimation of FA, MD, AD, and RD for all the ROIs in GM at age 300, 900, and 1500 days using the linear growth model. Overall changes from 300 to 1500 days are shown as percentages. The same scales were used for MD, AD, and RD to aid comparison with WM.

indispensable information for characterizing the developmental trajectories of brain maturation for rhesus monkeys, which are crucial as a baseline in investigating disease models of neuropathology and the effects of perturbations during early rearing and environmental insults. Because of the similarity in encephalization, the monkey provides the best model for

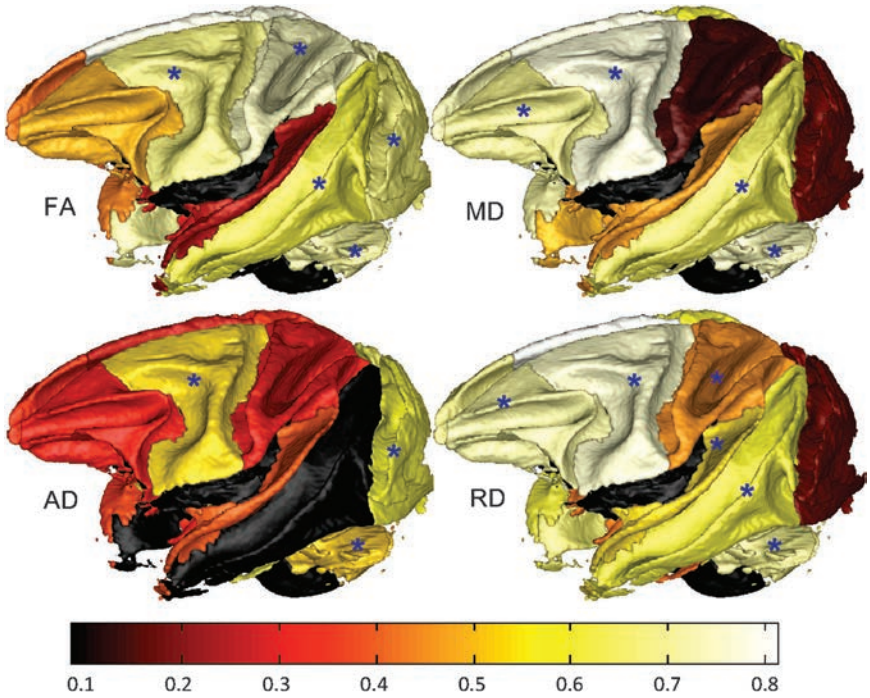

Figure 5. Correlations of diffusion property changes between WM and GM. Corresponding regions in left and right hemispheres showed highly similar correlation values and *P* values. Regions that showed a significant *P* value (<5%) are indicated with *. Note that color scales were chosen to represent the correlation values between the minimum and the maximum and not 0 to 1. Additionally, regions characterized by only WM or GM (e.g., CC, PM, and IL) were shown in black as correlations were impossible to calculate.

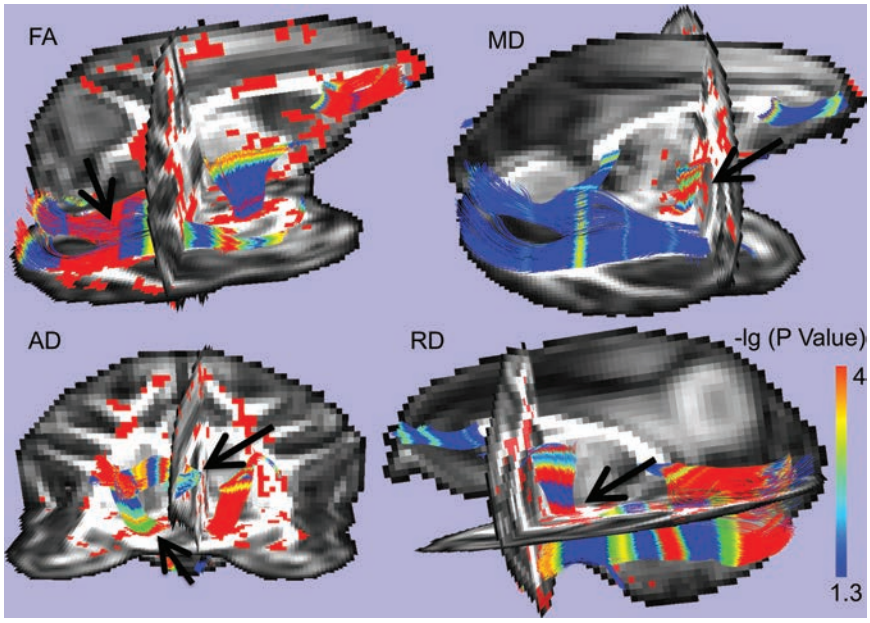

Figure 6. Overlay of results from fiber tract–based and VBA approaches showed consistency of significant findings. Voxels with significant DTI change across time (*P* values $<$ 0.05) from VBA are highlighted (as red voxels) in the 3D slices while segments of the fiber tracts *P* values $<$ 0.05 ($-$lg (*P* value) $>$ 1.3) from fiber tract analysis are highlighted with the chosen colormap. Arrows point to illustrative regions where significant changes were found consistently with both analyses.

comparison with human development. Three complementary approaches, ROI, voxel-wise, and tract-based were used to characterize developmental changes in WM. DTI properties (FA, MD, AD, and RD) revealed critical information reflective of WM integrity as well as offered insights into GM development. Overall, all the DTI properties indicated that there were major maturational changes in both WM and GM over this time period, demonstrating DTI properties provide important descriptors for neural development across the pre-to post-pubertal transition into adulthood.

FA has been commonly used to characterize brain development in DTI-based studies due to its sensitivity for detecting microstructural changes, as it is associated with both parallel and perpendicular diffusion. One drawback, however,

is that FA lacks the ability to pinpoint the exact process causing the changes. We were able to elucidate a more detailed description of the changes by including additional diffusion parameters, that is, MD, AD, and RD. Previous studies have mostly used FA to index the myelination process of WM (Morriss et al. 1999; Barkovich 2000). However, the mechanisms responsible for observed changes in FA are complicated and may also confer information about cell packing density, axon diameter, and organization (Beaulieu 2002; Mori and Zhang 2006; Wozniak and Lim 2006; Tamnes et al. 2010). AD reflects parallel diffusion, that is, diffusion along the fiber bundles, which has been associated with local organization of the tissue, including cell density, water content, intra-and extracellular water ratio (Ashtari et al. 2007), whereas RD reflects perpendicular diffusivity and is believed to be linked closely to the myelination of the axons (Zhang et al. 2009), as the myelin sheath is the major contributor to restrictive diffusion. Changes in both parallel and perpendicular diffusivity, that is, AD and RD, contribute to changes in FA and MD as a result of this complex interplay of biochemical and biophysical properties.

For the WM, we observed an overall increase in FA and AD along with a decrease in MD and RD in most brain regions and tracts. These changes were more prominent early in the development (300–900 days) and tapered off over time. ROI-based analysis showed a significant increase in FA and AD and a substantial decrease in RD in all the regions. It also showed a moderate decrease in MD in most of the lobes except for the posterior regions, the temporal lobes, and the pons and medulla, which stayed relatively stable. Tract-based analysis showed an overall significant increase in FA for all the examined tracts along with an increase in AD and a decrease in RD in most of the tracts. MD showed overall significant changes for most of the tracts but not a dominant trend, that is, some showed an increase while others a decrease. In addition, different "segments" along the fiber tracts showed some variations in the patterns of changes across time. These segments overlapped with the results from the voxel-wise analysis as well (Fig. 6). The findings from the 3 approaches were generally consistent. For example, the largest increases were found in the cingulate, the temporal visual and occipital lobe, and the corpus callosum from the ROI-based analysis, while the fiber tracts that run through these regions also reflected a vast increase in FA from the tract-based analysis, that is, the genu, splenium (they connect through the corpus callosum), and the segment of internal capsule tracts that connect to the temporal regions. Furthermore, the decrease of RD was more profound in the splenium between 300 and 900 days when compared with the genu where most of the changes occurred between 900 and 1500 days. Similarly, we observed more changes of RD at younger ages in the occipital lobe when compared with the frontal/prefrontal lobe.

One limitation of the study is the age range of the subjects, which started with the older weaned infant rather than from birth. The monkey brain matures quickly, and considerable development and myelination of some regions has already occurred by birth. In terms of overall size, the monkey brain is already 60% of adult volume at delivery, and some cortical regions are of adult size by 1 year of age. In the current study, regions with highest diffusion change are thus likely to be late maturing lobes. On the other hand, both the cerebellum and the temporal limbic lobe showed comparatively little change over time in diffusion properties, indicating that they have most likely gone through their substantial WM development before the neuroimaging had commenced. Younger monkeys should be included in the future studies to examine other critical features of earlier development during the neonatal period.

Table 2
Global *P* values of changes in diffusion properties along different fiber tracts

Tract name	FA	MD	AD	RD
Genu	**	*	NS	**
ILF L	**	*	**	**
ILF R	**	*	**	**
Cingulum L	**	**	**	**
Cingulum R	**	**	**	**
IntCap thalamus-anterior L	**	*	**	**
IntCap thalamus-anterior R	**	NS	**	**
IntCap thalamus-parietal L	**	**	**	**
IntCap thalamus-parietal R	**	**	**	**
IntCap pons-anterior L	**	NS	*	NS
IntCap pons-anterior R	**	**	**	**
IntCap pons-parietal L	**	NS	NS	NS
IntCap pons-parietal R	**	**	**	**
Splenium	**	**	**	**

Note: NS represents non-significant changes. Left and right hemispheres are designated using L and R. Internal capsule fibers (IntCap) include subdivisions connecting the thalamus to the anterior and parietal regions and pons to the anterior and parietal regions. ILF is the inferior longitudinal fasciculus.
P values smaller than or equal to 0.01 are indicated by **, and *P* values greater than 0.01 but smaller than or equal to 0.05 are noted by *.

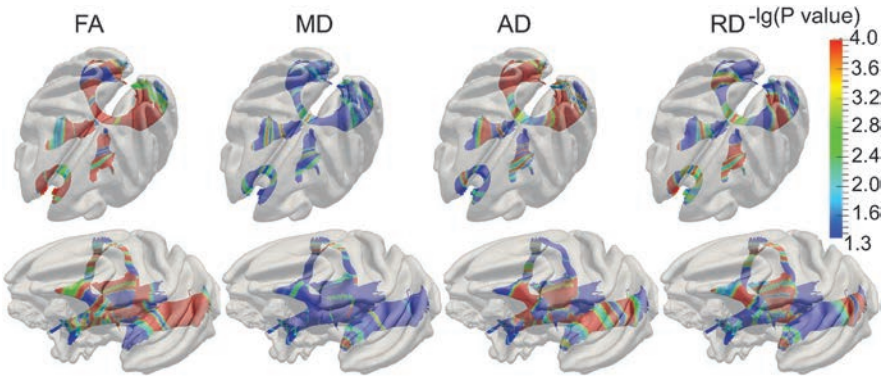

Figure 7. Significance fiber maps for change across time: FRATS-based *P* values are mapped along fiber tracts. Colormap was chosen to highlight regions with significant changes over time (*P* value < 0.05).

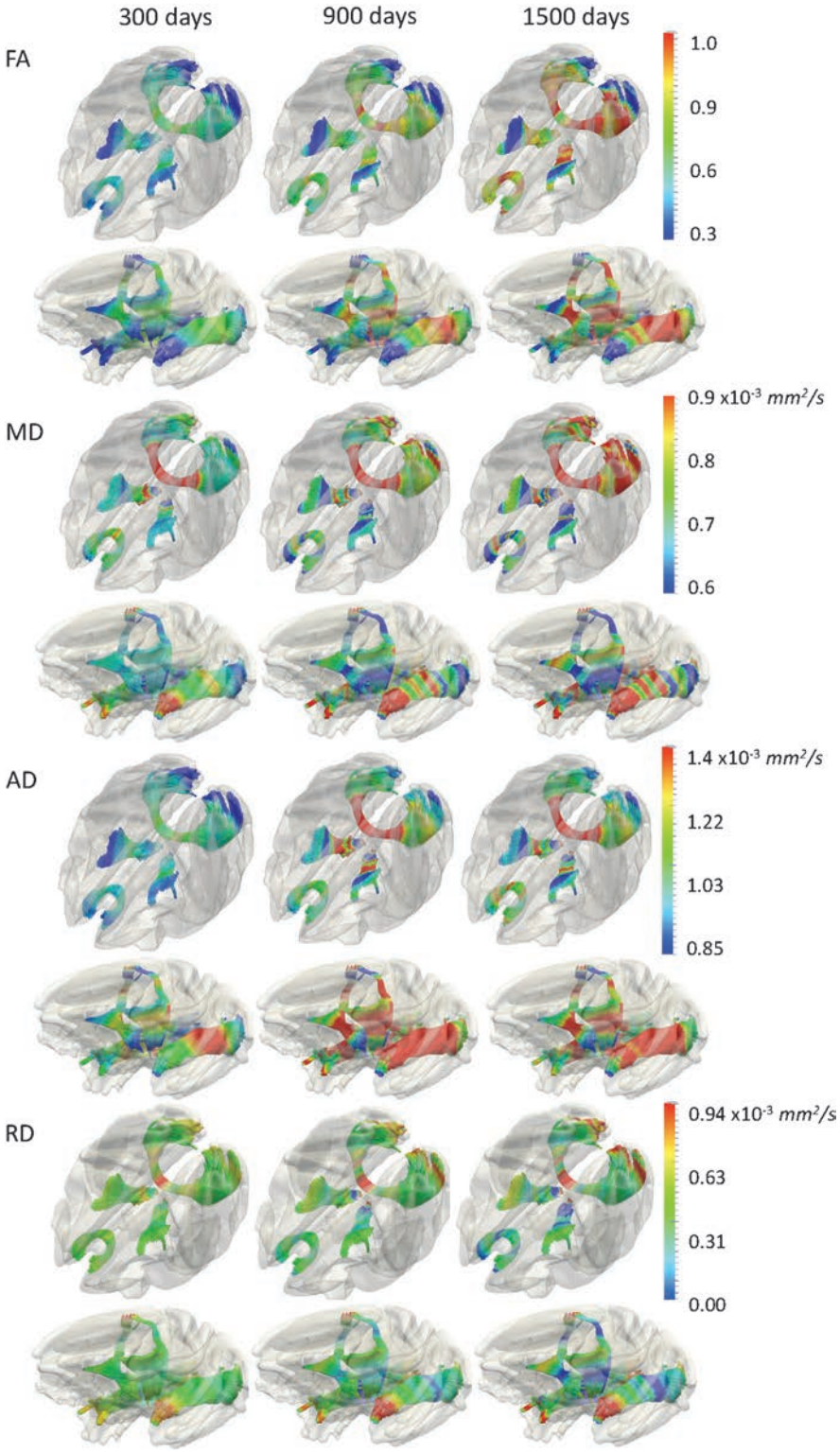

Figure 8. Diffusion properties along the fiber tract were estimated using the developmental data obtained at 300, 900, and 1500 days of age.

Diffusion properties of GM were also included in the ROI-based analysis. Studies that focus on the change of diffusion properties in GM during development are very limited; therefore, interpretation of this information is more open to debate. While GM maturation is a very complicated process, we hypothesize that the major causes of diffusion property changes emerge from the pruning process of dendritic connections, and the development of cortical parallel fibers and myelination of the WM fiber tracts that originate from or arrive at cortical terminals. In this study, AD was relatively stable in most regions, yet showed an increase in the temporal and occipital lobe as well as the cerebellum. Additionally, RD

showed an overall decrease in all the regions except for the occipital lobe. These changes in AD and RD were also reflected in the observed increase in FA and decrease in MD for most regions. Increase in AD most likely reflected the pruning process as it orchestrates the local organization of the GM tissue. Reductions in RD on the other hand, most likely resulted from myelination of WM fibers that start or end in the GM tissues.

It should be highlighted that we found strong correlations between the patterns of WM and GM changes for all diffusion properties in most brain regions, except for AD. Changes in FA and MD are linked to the interplay of changes in AD and RD. RD underwent substantial changes compared with AD, thus was primarily driving the changes observed in FA and MD. As a result, the changes of FA, MD, and RD were all mostly caused by the myelination process of the WM tracts either in the WM regions or in the GM regions they connect. Thus, those changes show strong correlations, whereas AD changes in WM and GM possibly resulted from different physiological processes as previously discussed (reorganization of axons in WM while pruning in GM). Additionally, we observed a delay of GM maturation compared with WM. As shown in Figure 2, most of the diffusion property changes occurred between 1 and 3 years in WM as compared with 3–5 years in GM. These findings are also consistent with human studies across a comparable age range (late infancy to early adulthood) (Lebel et al. 2008). Overall, analysis of FA, MD, AD, and RD together revealed that myelination processes were the likely main driven force in all diffusion property changes during this time (Snook et al. 2005; Giorgio et al. 2008, 2010). As a result, RD decreased in both WM and GM, which led to increases in FA and the decrease in MD.

Similar to findings in human studies (Buchel et al. 2004; Gong et al. 2005), we also observed hemispheric asymmetry in both ROI (WM and GM) and tract-based analyses. This observation was not surprising considering that the left and right hemispheres of the brain differ functionally and likely mature along slightly different developmental trajectories. Sex differences have been reported in several studies for both human (Giedd et al. 1999; De Bellis et al. 2001; Schmithorst et al. 2002; Lenroot et al. 2007) and nonhuman primates. However, we did not observe any significant difference between the 2 sexes. This lack of effect are likely the result of the limited sample size because it is known that male monkeys have larger brains than females and further that their brain continue to grow after puberty, whereas the females typically reach asymptote by menarche. As gender was semi-balanced across the age distribution (14 males and 11 females), we believe that the general developmental patterns described here are applicable to both males and females. Nevertheless, gender-specific patterns may exist that this study was unable to uncover.

It should also be noted that results from our studies revealed many similarities in brain maturation between rhesus monkeys and humans despite the fact that exact comparisons were challenging to perform due to different experimental setting, methodologies, and subject age ranges. WM showed most marked age effects for the CC as well as stronger effects in the temporal and occipital areas than in the frontal and parietal areas across the age range of 3 weeks to 19 years in humans (Lobel et al. 2009). Similarly, in our ROI-based results, the greatest increases in FA were found in the TV, OC, and the CC. We also saw marked changes in the CG, a region which was not specifically investigated in the Lobel study (Lobel et al. 2009). Furthermore, the temporal pattern of changes found in our study are in agreement to what was reported across corresponding age range in humans (Lobel et al. 2009), which is more rapid at younger ages and tapers off going into adulthood. In determining the driving force for changes in FA, several similar studies (Qiu et al. 2008; Lobel et al. 2009; Verhoeven et al. 2010) in humans reported that RD instead of AD was playing the major role as it reflects mostly the myelination process. This also agrees with what we found in the rhesus monkeys. However, AD seems to play more of a role in monkeys than in humans, given that we saw significant AD increases in many brain regions while decreased AD was reported in similar human studies (Qiu et al. 2008; Verhoeven et al. 2010). This could indicate that different under biological changes occur in monkeys and humans as the brain matures that are reflected in different changes of AD.

In conclusion, brain maturation is a long process that spans from infancy to adulthood. This study presented for the first time the normative developmental trajectories of primate brains from late infancy to young adulthood with DTI. Diffusion properties that provide important indices of brain maturation showed significant overall change with age. Most of findings are similar to those from human studies, although a few followed unique patterns. This information is particularly crucial as rhesus monkeys are important animal models for the investigation of normal brain neurodevelopment as well as for several neurodevelopmental disorders, including autism, attention deficit hyperactivity disorder, and schizophrenia in humans (Machado and Bachevalier 2003).

Funding

National Science Foundation (BCS-08-26844 to H.Z.); the National Institutes of Health (UL1-RR025747-01 to H.Z., MH086633 to H.Z., AG 033387 to H.Z., P01 CA142538-01 to H.Z., AI067518 to C.L.C., J.H.G., Y.S., HD039386 to C.L.C., P50 MH064065 to J.H.G., M.A.S., MH070890 to J.H.G., M.A.S., HD053000 to J.H.G., T32 MH019111-13 to R.C.K., K01 MH083045-01 to R.C.K., T32 HD40127 to R.C.K., Roadmap Grant U54 EB005149-01 to M.A.S., P50 MH078105-01A2S1 to Y.S., M.A.S. RR025747-01, P01CA142538-01, MH086633, EB005149-01 and AG033387 to H.Z., J.W.); and the UNC Intellectual and Developmental Disabilities Research Center (P30 HD03110 to M.A.S., S.J.S., R01 MH091645 to M.A.S.).

Notes

We thank Dr Sarang Joshi and Dr Brad Davis for providing us with the atlas building tool, atlaswerks (Joshi et al. 2004). *Conflict of Interest* : None declared.

References

Adluru N, Zhang H, Fox AS, Shelton SE, Ennis MC, Bartosic AM, Oler JA, Tromp DPM, Zakszewski E, Gee JC, et al. 2012. A diffusion tensor brain template for rhesus macaques. Neuroimage. 59(1):306–318.

Alexander D, Pierpaoli C, Basser P, Gee J. 2001. Spatial transformations of diffusion tensor magnetic resonance images. IEEE Trans Med Imaging. 20(11):1131–1139.

Amaral DG. 2002. The primate amygdala and the neurobiology of social behavior: implications for understanding social anxiety. Biol Psychiatry. 51(1):11–17.

Ashtari M, Cervellione KL, Hasan KM, Wu J, McIlree C, Kester H, Ardekani BA, Roofeh D, Szeszko PR, Kumra S. 2007. White matter development during late adolescence in healthy males: a cross-sectional diffusion tensor imaging study. Neuroimage. 35(2):501–510.
Barkovich AJ. 2000. Concepts of myelin and myelination in neuroradiology. Am J Neuroradiol. 21(6):1099–1109.
Barr CS, Goldman D. 2006. Review: non-human primate models of inheritance vulnerability to alcohol use disorders. Addict Biol. 11(3–4): 374–385.
Beaulieu C. 2002. The basis of anisotropic water diffusion in the nervous system—a technical review. NMR Biomed. 15(7–8): 435–455.
Bennett AJ. 2008. Gene environment interplay: nonhuman primate models in the study of resilience and vulnerability. Dev Psychobiol. 50(1):48–59.
Buchel C, Raedler T, Sommer M, Sach M, Weiller C, Koch MA. 2004. White matter asymmetry in the human brain: a diffusion tensor MRI study. Cereb Cortex. 14(9):945–951.
Corouge I, Fletcher PT, Joshi S, Gouttard S, Gerig G. 2006. Fiber tract-oriented statistics for quantitative diffusion tensor MRI analysis. Med Image Anal. 10(5):786–798.
Croxson PL, Johansen-Berg H, Behrens TEJ, Robson MD, Pinsk MA, Gross CG, Richter W, Richter MC, Kastner S, Rushworth MFS. 2005. Quantitative investigation of connections of the prefrontal cortex in the human and macaque using probabilistic diffusion tractography. J Neurosci. 25(39):8854–8866.
D'Arceuil HE, Westmoreland S, de Crespigny AJ. 2007. An approach to high resolution diffusion tensor imaging in fixed primate brain. Neuroimage. 35(2):553–565.
Dauguet J, Peled S, Berezovskii V, Delzescaux T, Warfield SK, Born R, Westin CF. 2006. 3D histological reconstruction of fiber tracts and direct comparison with diffusion tensor MRI tractography. Proceedings of the MICCAI 2006 Lecture Notes Computer Science 4190; Copenhagen, Denmark. Berlin (Germany): Springer-Verlag. p. 109–116.
Dauguet J, Peled S, Berezovskii V, Delzescaux T, Warfield SK, Born R, Westin CF. 2007. Comparison of fiber tracts derived from in-vivo dti tractography with 3d histological neural tract tracer reconstruction on a macaque brain. Neuroimage. 37:530–538. 2007.
Dawson G, Fischer K. 1994. Human behavior and the developing brain. New York: Guilford Press.
De Bellis MD, Keshavan MS, Beers SR, Hall J, Frustaci K, Masalehdan A, Noll J, Boring AM. 2001. Sex differences in brain maturation during childhood and adolescence. Cerebral Cortex. 11(6):552–557.
Ding Z, Gore JC, Anderson AW. 2003. Classification and quantification of neuronal fiber pathways using diffusion tensor MRI. Magn Reson Med. 49:716–721.
Engert F, Bonhoeffer T. 1999. Dendritic spine changes associated with hippocampal long-term synaptic plasticity. Nature. 399:66–70.
Fletcher P, Tao R, Jeong WK, Whitaker R. 2007. A volumetric approach to quantifying region-to-region white matter connectivity in diffusion tensor MRI. Proceedings of the Information Processing in Medical Imaging (IPMI) 2007 Lecture Notes Computer Science 4584; Kerkrade, the Netherlands. Berlin (Germany): Springer-Verlag. p. 346–358.
Genovese CR, Lazar NA, Nichols T. 2002. Thresholding of statistical maps in functional neuroimaging using the false discovery rate. Neuroimage. 15(4):870–878.
Giedd JN, Blumenthal J, Jeffries NO, Castellanos FX, Liu H, Zijdenbos A, Paus T, Evans AC, Rapoport JL. 1999. Brain development during childhood and adolescence: a longitudinal MRI study. Nat Neurosci. 2(10):861–863.
Giorgio A, Watkins K, Chadwick M, James S, Winmill L, Douaud G, Stefano ND, Matthews P, Smith S, Johansen-Berg H, et al. 2010. Longitudinal changes in grey and white matter during adolescence. Neuroimage. 49(1):94–103.
Giorgio A, Watkins K, Douaud G, James A, James S, Stefano ND, Matthews P, Smith S, Johansen-Berg H. 2008. Changes in white matter microstructure during adolescence. Neuroimage. 39(1):52–61.
Glatzel M, Pekarik V, Luhrs T, Dittami J, Aguzzi A. 2002. Analysis of the prion protein in primates reveals a new polymorphism in codon 226 (y226f). Biol Chem. 383(6):1021–1025.
Gong G, Jiang T, Zhu C, Zang Y, Wang F, Xie S, Xiao J, Guo X. 2005. Asymmetry analysis of cingulum based on scale-invariant parameterization by diffusion tensor imaging. Hum Brain Mapp. 24(2): 92–98.
Goodlett CB, Fletcher PT, Gilmore JH, Gerig G. 2009. Group analysis of DTI fiber tract statistics with application to neurodevelopment. Neuroimage. 45(Suppl 1):S133–S142, Mathematics in Brain Imaging.
Grant KA, Bennett AJ. 2003. Advances in nonhuman primate alcohol abuse and alcoholism research. Pharmacol Ther. 100(3):235–255.
Harlow HF, Harlow MK, Suomi SJ. 1971. From thought to therapy: lessons from a primate laboratory. Am Sci. 59(5):538–549.
Joshi S, Davis B, Jomier M, Gerig G. 2004. Unbiased diffeomorphic atlas construction for computational anatomy. Neuroimage. 23:S151–S160.
Knickmeyer RC, Styner M, Short SJ, Lubach GR, Kang C, Hamer R, Coe CL, Gilmore JH. 2010. Maturational trajectories of cortical brain development through the pubertal transition: unique species and sex differences in the monkey revealed through structural magnetic resonance imaging. Cereb Cortex. 20(5):1053–1063.
Lacreuse A, Herndon JG. 2009. Nonhuman primate models of cognitive aging. In: Bizon J, Woods A, editors. Animals models of human cognitive aging. New York: Humana Press. p. 29–58.
Lebel C, Walker L, Leemans A, Phillips L, Beaulieu C. 2008. Microstructural maturation of the human brain from childhood to adulthood. NeuroImage. 40(3):1044–1055.
Lebherz C, Maguire AM, Auricchio A, Tang W, Aleman TS, Wei Z, Grant R, Cideciyan AV, Jacobson SG, Wilson JM, et al. 2005. Nonhuman primate models for diabetic ocular neovascularization using aav2-mediated overexpression of vascular endothelial growth factor. Diabetes. 54(4):1141–1149.
Lenroot RK, Gogtay N, Greenstein DK, Wells EM, Wallace GL, Clasen LS, Blumenthal JD, Lerch J, Zijdenbos AP, Evans AC, et al. 2007. Sexual dimorphism of brain developmental trajectories during childhood and adolescence. Neuroimage. 36(4):1065–1073.
Li Y, Zhu H, Shen D, Lin W, Gilmore JH, Ibrahim JG. 2011. Multiscale adaptive regression models for neuroimaging data. J R Stat Soc Series B Stat Methodol. 73:559–578.
Liu Z, Zhu H, Marks B, Katz L, Goodlett C, Gerig G, Styner M. 2009. Voxel-wise group analysis of DTI. Proceedings of the IEEE International Symposium on Biomedical Imaging: From Nano to Macro. p. 807–810.
Lobel U, Sedlacik J, Gullmar D, Kaiser W, Reichenbach J, Mentzel H. 2009. Diffusion tensor imaging: the normal evolution of ADC, RA, FA, and eigenvalues studied in multiple anatomical regions of the brain. Neuroradiology. 51(4):253–263.
Lubach GR, Coe CL. 2006. Preconception maternal iron status is a risk factor for iron deficiency in infant rhesus monkeys (macaca mulatta). J Nutr. 136(9):2345–2349.
Machado CJ, Bachevalier J. 2003. Non-human primate models of childhood psychopathology: the promise and the limitations. J Child Psychol Psychiatry. 44(1):64–87.
Makris N, Papadimitriou GM, van der Kouwe A, Kennedy DN, Hodge SM, Dale AM, Benner T, Wald LL, Wu O, Tuch DS, et al. 2007. Frontal connections and cognitive changes in normal aging rhesus monkeys: a DTI study. Neurobiol Aging. 28(10): 1556–1567.
Mori S, Zhang J. 2006. Principles of diffusion tensor imaging and its applications to basic neuroscience research. Neuron. 51(5):527–539.
Morriss MC, Zimmerman RA, Bilaniuk LT, Hunter JV, Haselgrove JC. 1999. Changes in brain water diffusion during childhood. Neuroradiology. 41:929–934.
Parker GJM, Stephan KE, Barker GJ, Rowe JB, MacManus DG, Wheeler-Kingshott CAM, Ciccarelli O, Passingham RE, Spinks RL, Lemon RN, et al. 2002. Initial demonstration of in vivo tracing of axonal projections in the macaque brain and comparison with the human brain using diffusion tensor imaging and fast marching tractography. Neuroimage. 15(4):797–809.
Qiu D, Tan LH, Zhou K, Khong PL. 2008. Diffusion tensor imaging of normal white matter maturation from late childhood to young adulthood: voxel-wise evaluation of mean diffusivity, fractional anisotropy, radial and axial diffusivities, and correlation with reading development. Neuroimage. 41(2):223–232.

Rueckert D, Sonod LI, Hayes C, Hill DL, Leach MO, Hawkes DJ. 1999. Nonrigid registration using free-form deformations: application to breast MR images. IEEE Trans Med Imaging. 18(8):712–721.

Schmithorst VJ, Wilke M, Dardzinski BJ, Holland SK. 2002. Correlation of white matter diffusivity and anisotropy with age during childhood and adolescence: a cross-sectional diffusion-tensor MR imaging study1. Radiology. 222(1):212–218.

Segerstrom SC, Lubach GR, Coe CL. 2006. Identifying immune traits and biobehavioral correlates: generalizability and reliability of immune responses in rhesus macaques. Brain Behav Immun. 20(4): 349–358.

Short SJ, Lubach GR, Karasin AI, Olsen CW, Styner M, Knickmeyer RC, Gilmore JH, Coe CL. 2010. Maternal influenza infection during pregnancy impacts postnatal brain development in the rhesus monkey. Biol Psychiatry. 67(10):965–973.

Snook L, Paulson LA, Roy D, Phillips L, Beaulieu C. 2005. Diffusion tensor imaging of neurodevelopment in children and young adults. Neuroimage. 26(4):1164–1173.

Stepanyants A, Hof PR, Chklovskii DB. 2002. Geometry and structural plasticity of synaptic connectivity. Neuron. 34(2):275–288.

Styner M, Knickmeyer R, Coe C, Short SJ, Gilmore J. 2008. Automatic regional analysis of DTI properties in the developmental macaque brain. Proceedings of the SPIE Medical Imaging: Image Processing 6914; San Diego, CA. Berlin (Germany): Springer-Verlag. p. 89–91.

Styner M, Knickmeyer R, Joshi S, Coe C, Short SJ, Gilmore J, Pluim JPW, Reinhardt JM. 2007. Automatic brain segmentation in rhesus monkeys. In Proceedings of the SPIE Medical Imaging 6512. p. 65122 L1–65122 L8.

Sullivan EV, Sable HJ, Strother WN, Friedman DP, Davenport A, Tillman-Smith H, Kraft RA, Wyatt C, Szeliga KT, Buchheimer NC, et al. 2005. Neuroimaging of rodent and primate models of alcoholism: initial reports from the integrative neuroscience initiative on alcoholism. Alcohol Clin Exp Res. 29(2):287–294.

Tamnes CK, Østby Y, Fjell AM, Westlye LT, Due-Tønnessen P, Walhovd KB. 2010. Brain maturation in adolescence and young adulthood: regional age-related changes in cortical thickness and white matter volume and microstructure. Cereb Cortex. 20(3):534–548.

Verhoeven JS, Sage CA, Leemans A, Van Hecke W, Callaert D, Peeters R, De Cock P, Lagae L, Sunaert S. 2010. Construction of a stereotaxic DTI atlas with full diffusion tensor information for studying white matter maturation from childhood to adolescence using tractography-based segmentations. Hum Brain Mapp. 31(3):470–486.

Williams R, Bokhari S, Silverstein P, Pinson D, Kumar A, Buch S. 2008. Nonhuman primate models of neuroaids. J Neurovirol. 14(4):292–300.

Wozniak JR, Lim KO. 2006. Advances in white matter imaging: a review of in vivo magnetic resonance methodologies and their applicability to the study of development and aging. Neurosci Biobehav Rev. 30(6):762–774.

Yushkevich P, Piven J, Cody Hazlett H, Gimpel Smith R, Ho S, Gee J, Gerig G. 2006. User-guided 3D active contour segmentation of anatomical structures: significantly improved efficiency and reliability. Neuroimage. 31:1116–1128.

Zhang J, Jones M, DeBoy CA, Reich DS, Farrell JAD, Hoffman PN, Griffin JW, Sheikh KA, Miller MI, Mori S, et al. 2009. Diffusion tensor magnetic resonance imaging of Wallerian degeneration in rat spinal cord after dorsal root axotomy. J Neurosci. 29(10): 3160–3171.

Zhu H, Kong L, Li R, Styner M, Gerig G, Lin W, Gilmore JH. 2011. FADTTS: functional analysis of diffusion tensor tract statistics. NeuroImage. 56(3):1412–1425.

Zhu H, Li Y, Ibrahim J, Lin W, Shen D. 2009. MARM: multiscale adaptive regression models for neuroimaging data. Proceedings of the Information Processing in Medical Imaging (IPMI) 2009 Lecture Notes Computer Science 21; Williamsburg, VA. Berlin (Germany): Springer-Verlag. p. 314–325.

Zhu H, Styner M, Tang N, Liu Z, Lin W, Gilmore J. 2010. FRATS: functional regression analysis of DTI tract statistics. IEEE Trans Med Imaging. 29(4):1039–1049.